Controlling the Charge State of Individual Gold Adatoms

Jascha Repp,[1]* Gerhard Meyer,[1] Fredrik E. Olsson,[2] Mats Persson[2]

The nature and control of individual metal atoms on insulators are of great importance in emerging atomic-scale technologies. Individual gold atoms on an ultrathin insulating sodium chloride film supported by a copper surface exhibit two different charge states, which are stabilized by the large ionic polarizability of the film. The charge state and associated physical and chemical properties such as diffusion can be controlled by adding or removing a single electron to or from the adatom with a scanning tunneling microscope tip. The simple physical mechanism behind the charge bistability in this case suggests that this is a common phenomenon for adsorbates on polar insulating films.

The chemical and physical properties of ions in general are qualitatively different from those of the corresponding neutral atoms. Thus, the ability to switch between different charge states of atoms could lead to control of their properties. In a chemical oxidation, reduction, or redox reaction, the charge state of atoms is controlled by the reactants and the chemical environment (*1*). At surfaces, the charge state of an adatom is determined by the choice of substrate and coadsorbates. The capabilities of the scanning tunneling microscope (STM) to image, characterize, and manipulate single atoms and molecules on surfaces (*2*–*4*) could enable switching between different charge states of individual adatoms on surfaces without changing the chemical environment.

We show that on a polar insulating surface, the charge state of individual adatoms can be controlled. We studied Au atoms adsorbed on ultrathin insulating NaCl films with a low-temperature STM. By positioning the STM tip above an Au adatom and applying a voltage pulse, the adatom can be reversibly switched between its neutral and negatively charged state. Most importantly, both states are stable, that is, an additional charge remains on the adsorbate until it is removed by a voltage pulse of reversed sign. We interpreted our results using density functional theory (DFT) calculations.

Our experiments were carried out with a home-built STM operated between 5 and 60 K. Cu(111) and Cu(100) single-crystal samples were cleaned by several sputtering and annealing cycles, upon which NaCl films were evaporated thermally. The substrate temperatures were kept at about 300 K so that defect-free (100)-terminated NaCl islands with two or more atomic layers were formed (*5*, *6*). Individual Au adatoms were adsorbed at a sample temperature of 5 to 10 K with the sample located in the STM. Bias voltages refer to the sample voltage with respect to the tip. An electrochemically etched W wire was used for the STM tip. All of the results shown here were obtained in experiments carried out on NaCl bilayers on Cu(111), but the results for the trilayer and for NaCl bi- and trilayers on Cu(100) were similar.

Individual Au adatoms on NaCl(100)/Cu(111) were imaged as protrusions (Fig. 1). The apparent height ranged from 2.0 Å for a tunneling current of $I \approx 10$ pA to 2.5 Å for $I \approx 0.2$ nA. The adsorption site was determined to be on top of the Cl^- ions directly from atomically resolved STM images of the Cl^- ions (*7*), as well as indirectly from the adatom position with respect to artificially created Cl vacancies (*8*).

By applying a voltage pulse, we could manipulate the adsorption state of an individual Au adatom, as revealed in Fig. 1, A to D, by the change of tunneling conductance and appearance in the STM image. In the adatom manipulation, the tip was first positioned directly above an Au adatom. The feedback loop was then switched off, and a positive voltage $V \geq 0.6$ V was applied. After a time t, which depended on the specific tunneling parameters, a sharp current drop by about a factor of 3 was observed. In subsequent images, the corresponding Au adatom appeared different but still was located at the same position. The image of the manipulated Au adatom is characterized by a sombrero-like shape with an ~0.5 Å smaller protrusion than that in the image of the original state surrounded by a depression. By applying a negative voltage pulse of about −1 V, we could switch the manipulated adatom back to its original state. Two different experimental observations suggest that an Au adatom in its original state is neutral, whereas after manipulation it is negatively charged.

In the first experiment, the two-dimensional electron gas in the interface state (IS) band of NaCl/Cu(111) (*6*) was used as a probe to characterize the two different states of the Au adatoms. The STM images in Fig. 1, E and F, reveal that scattering of the IS electrons from the adatoms could be observed for the manipulated adatoms only. As the probability density of the interface electrons falls off to almost zero at the position of the Au adatoms (*6*), the short-range potential of a neutral Au adatom should be a weak scatterer of the IS electrons. A charged Au adatom, however, results in a long-range electrostatic potential that should strongly scatter the IS electrons below the adatom. Thus, this observation suggests that the manipulated Au adatom is charged.

In the second experiment, the Au adatom charge state was probed by the direct interaction of the adatom with a biased tip. When a bias voltage of about 1 V was applied and the tip laterally approached to the position of a manipulated Au adatom, the adatom moved away from the negatively charged tip. At lower or negative bias voltages, the adatom was often picked up by the STM tip. This observation suggests that the manipulated Au adatoms were negatively charged.

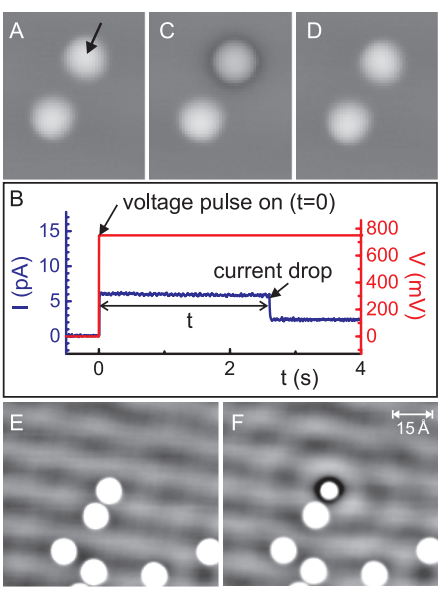

Fig. 1. Example of the manipulation of the Au adatom state. After recording the image (**A**), the STM tip was positioned above one of the Au adatoms (arrow) and a positive voltage pulse was applied to the sample. After a time t, a sharp decrease in the tunneling current can be observed (**B**). A subsequent STM image (**C**) shows that the manipulated Au adatom has a different appearance but did not change its position. By applying a negative voltage pulse, one can switch the manipulated adatom back to its initial state (**D**). The Au adatoms in the initial state (**E**) do not scatter interface-state electrons of NaCl/Cu(111), whereas the manipulated adatom (**F**) acts as a scatterer.

[1]IBM, Zurich Research Laboratory, CH-8803 Rüschlikon, Switzerland. [2]Department of Applied Physics, Chalmers/Göteborg University, S-41296, Göteborg, Sweden.

*To whom correspondence should be addressed. E-mail: jre@zurich.ibm.com

The states of the original and the manipulated Au adatoms were both stable and must therefore be associated with two different geometric configurations of the adatom and the NaCl film. A simple electron transfer without any lasting changes of the ion-core positions would not be stable, because the electron residing in an excited state on the manipulated Au adatom would rapidly tunnel into the metal.

Experimentally, the behavior that we observed for Au adatoms on NaCl/Cu(100) was similar to that observed for NaCl/Cu(111). An Au adatom on NaCl/Cu(100) is also initially neutral and imaged as a large protrusion. It can similarly be switched to a negatively charged state with a sombrero-like appearance. However, switching back to the initial state was not possible on this surface. A deeper physical insight into the nature of these two states of the Au adatom and a corroboration of the assignment of the states to different charge states require a theoretical study of the adsorption and STM images of Au adatoms on a NaCl film supported by a Cu surface.

To this end, we carried out DFT calculations of this system using a plane-wave and projector-augmented-wave method as implemented in the VASP code (*9*, *10*). Because this method is based on a supercell geometry and the NaCl layers are incommensurate with the Cu(111) surface, this study was restricted to NaCl layers on a Cu(100) surface where the close 2:3 match of the NaCl and Cu lattice constants supports a commensurate structure (*11*). The main results presented here were obtained for a single Au atom on a NaCl bilayer supported by four Cu substrate layers. A relatively large, square surface unit cell accommodating 36 Cu atoms in each substrate layer was used in order to minimize adatom-adatom interactions (*12*). The Au adatom, the NaCl bilayer, and the two topmost Cu layers were structurally optimized. The simulations of the STM images were based on the Tersoff-Hamann approximation (*13*) and on the Kohn-Sham wave functions to determine surfaces of constant local density of states (LDOS) (*14*).

In agreement with our experiments, the theoretical investigation finds two different stable states for Au atoms in on-top sites of a Cl^- ion in the NaCl film on Cu(100). As suggested by the partial density of *s*-states in Fig. 2, one state (Au^0) is nearly neutral, whereas the other state (Au^-) of the Au adatom is negatively charged by one electron. For the Au^0 adatom, a weak bond is formed with a binding energy of 0.4 eV. The Au^0 adatom is adsorbed about 3.2 Å above the Cl^- ion and leaves the ionic positions within the NaCl film relatively unperturbed. As illustrated in Fig. 2, the position of the Au^- adatom is somewhat different, namely, 0.4 Å closer to the surface, and is stabilized by large ionic relaxations within the NaCl film. The Cl^- ion underneath the adatom is forced to move downward by 0.6 Å and the surrounding Na^+ ions to move upward by 0.6 Å. This relaxation pattern creates an attractive potential for the additional charge on the Au adatom (*15*). The Au^- state is further stabilized by the screening charge in the metal substrate (i.e., positive image charge) (*16*) and by the electronic polarization of the ionic layer, resulting in an adsorption energy of 1.1 eV. In fact, the partially occupied Au(6*s*) state of the Au^0 adatom at the Fermi level (E_F) is shifted downward by 1.0 eV and becomes fully occupied for the Au^- adatom.

To establish a direct link between experiment and theory for the two different charge states of the Au adatoms, we calculated the corresponding STM images shown in Fig. 2. In agreement with experiments, the calculated image of the Au^0 adatom on NaCl/Cu(100) shows simply a large protrusion, whereas the calculated image of the Au^- adatom has a sombrero-like appearance (*17*). This agreement supports the assignment of the charge states of the initial and manipulated Au adatom in the experiments.

The physical mechanism behind the switching between the two different charge states of the Au adatom is attributed to inelastic electron tunneling (IET) (*18*–*20*). We find evidence of a new IET mechanism in the situation in which an insulating film reduces the coupling of the electronic states of the adatom with the metal substrate dramatically. The data suggest that the coupling is so weak that the lifetime of a negative ion resonance (NIR) state of the adatom is in the range of the ionic vibrational periods, which results in a capture of the tunneling electrons. An electron, tunneling resonantly into the NIR state, remains there for a sufficiently long time so that the adatom and its surrounding ions have time to relax for the NIR state to be shifted below E_F, and the electron is captured. This mechanism results in a quantum yield (i.e., the probability of a switching event per tunneling electron) on the order of unity. This high yield cannot be directly observed because of the inability to measure a current pulse consisting of only a few electrons.

Instead, we determined the distance Δz that the tip has to be retracted from an initial position z_0, corresponding to I_0 = 10 pA at V_0 = 0.5 V, to observe a mean switching time of 1 s. The result of this statistical analysis (Fig. 3) reveals that below 1.4 V, Δz increases linearly with voltage, and that for higher voltages, a saturation is observed. This saturation rules out the possibility that the electric field in the tunneling junction is responsible for the switching. To estimate the quantum yield at saturation, i.e., for Δz = 10.5 Å and V = 1.4 V, the tunneling current I needs to be extrapolated from I_0 = 10 pA at Δz = 0 Å and V_0 = 0.5 V. Using an exponential extrapolation of I with Δz yields a decrease of about 10 orders of magnitude, which was quantified using an $I(z)$ measurement at higher currents. There should also be a

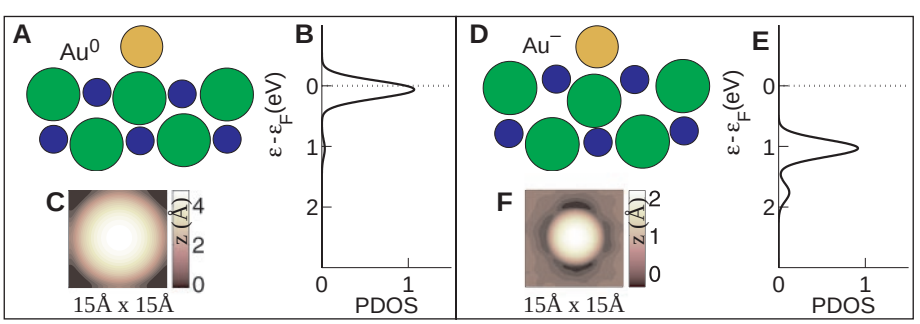

Fig. 2. Calculated electronic and geometric properties of the neutral (**A** to **C**) and negatively charged (**D** to **F**) Au adatom. The ion-core positions are represented by a sphere model (A and D), in which the spheres representing Au, Cl^-, and Na^+ are colored gold, green, and blue, respectively. The calculated partial density of states (PDOS) of *s*-states at the Au adatom (B and E) is presented using the energy broadening set by the Fermi level smearing used in the calculation (*26*). The 6*s*-derived state is partially and fully occupied in (B) and (E), respectively. STM images are simulated by contours of constant LDOS (C and F), where z = 0 Å corresponds to a distance of 6.4 Å from the topmost NaCl reference plane (*17*).

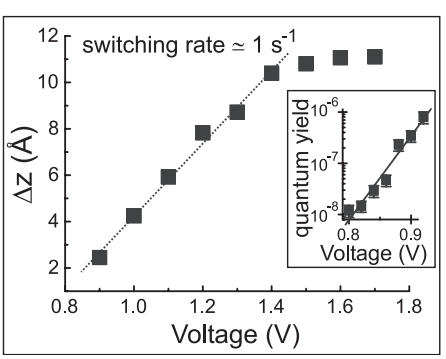

Fig. 3. Statistical analysis of the switching behavior of Au adatoms on an NaCl bilayer on Cu(111). For different voltages in the range of 0.9 to 1.7 V, the tip was retracted by Δz from its initial position z_0 corresponding to I_0 = 10 pA at V_0 = 500 mV, such that a mean switching time of 1 s could be observed. A saturation is observed at higher voltages, whereas below 1.4 V, Δz increases linearly with voltage (line fit). For voltage pulses <0.9 V, the quantum yield is sufficiently low that it can be determined directly by measuring the current (**inset**).

dramatic increase of the tunneling current with increasing voltage because of tunneling through the NIR state (*21*). Based on $I(V)$ measurements for other adsorbates on NaCl films, we estimate that tunneling through the NIR state increases the tunneling current by about two orders of magnitude. The extrapolation of I to $\Delta z = 10.5$ Å and $V = 1.4$ V thus gives a current on the order of one electron per second, corresponding to a quantum yield on the order of unity. This extremely high yield is consistent with a capture of electrons tunneling into the NIR state. Further support for this interpretation comes from the experimentally suggested position of a resonance level at $E_{NIR} = 1.4$ eV above E_F or 2.6 eV below the vacuum level (*22*), which is close to the electron affinity of an isolated Au atom of 2.3 eV (below the vacuum level). Finally, for V smaller than 0.9 V, the quantum yield can be measured directly and increases exponentially with increasing voltage (Fig. 3, inset). This exponential increase is consistent with the observed linear increase of Δz at voltages well below the NIR state.

The difference in physical properties of the two states is documented in diffusion experiments. Interestingly, the two differently charged states of the Au adatom are conserved during the diffusion process. In the Au^0 state, adatom diffusion sets in at a temperature of about 60 K, whereas in the Au^- state the adatoms already diffuse at a lower temperature of 40 K. This difference even allows the diffusion of single Au adatoms to be switched on and off.

Small clusters of Au adatoms can similarly be switched between different charge states, which was demonstrated in an experiment for Au dimers and trimers on NaCl films. Nanometer-sized Au clusters on insulators have been shown to be catalytically active by partial electron transfer from color centers (*23*). This finding opens up the possibility of switching surface catalytic reactions on and off by manipulating the charge state of individual nanometer-sized Au clusters. The switching between the two differently charged states also suggests their use as a nonvolatile memory device at the ultimate spatial limit.

Associated with the control of the charge state of the Au adatom is the control of its magnetic moment. In the Au^0 adatom, the 6*s*-derived state is partially occupied, resulting in a net (spin) magnetic moment, whereas in the Au^- adatom this state is fully occupied and the adatom is nonmagnetic. This moment is expected to be paramagnetic because the magnetic-anisotropy energy of the Au(6*s*)-derived state should be minimal. However, a paramagnetic moment that is decoupled from a metal substrate by an insulating film might be of some interest in quantum-information processing.

References and Notes

1. L. C. Pauling, *The Nature of the Chemical Bond* (Cornell Univ. Press, Ithaca, NY, 1939).
2. D. M. Eigler, E. K. Schweizer, *Nature* **344**, 524 (1990).
3. D. M. Eigler, C. P. Lutz, W. E. Rudge, *Nature* **352**, 600 (1991).
4. T.-C. Shen *et al*., *Science* **268**, 1590 (1995).
5. R. Bennewitz *et al*., *Surf. Sci.* **438**, 289 (1999).
6. J. Repp, G. Meyer, K.-H. Rieder, *Phys. Rev. Lett.* **92**, 036803 (2004).
7. Only the Cl^- ions are imaged as protrusions (*8*, *11*, *24*, *25*).
8. J. Repp, S. Fölsch, G. Meyer, K.-H. Rieder, *Phys. Rev. Lett.* **86**, 252 (2001).
9. G. Kresse, J. Furthmüller, *Phys. Rev. B* **54**, 11169 (1996).
10. G. Kresse, D. Joubert, *Phys. Rev. B* **59**, 1758 (1999).
11. F. E. Olsson, M. Persson, *Surf. Sci.* **540**, 172 (2003).
12. The vacuum region was 20 Å. The surface Brillouin zone was sampled by 2×2 *k*-points.
13. J. Tersoff, D. R. Hamann, *Phys. Rev. Lett.* **50**, 1998 (1983).
14. F. E. Olsson, M. Persson, N. Lorente, L. J. Lauhon, W. Ho, *J. Phys. Chem. B* **106**, 8161 (2002).
15. A. L. Shluger, A. M. Stoneham, *J. Phys. Condens. Matter* **5**, 3049 (1993).
16. M. Stoneham, P. W. Tasker, *J. Phys. C* **18**, L543 (1985).
17. The simulated STM images reproduce all features of the experimental appearance. However, a quantitative comparison of the images of Au^0 suffers from the limited ability of DFT to describe the NIR state by Kohn-Sham states.
18. G. P. Salam, M. Persson, R. E. Palmer, *Phys. Rev. B* **49**, 10655 (1994).
19. S. Gao, M. Persson, B. I. Lundqvist, *Solid State Commun.* **84**, 271 (1992).
20. C. Stipe *et al*., *Phys. Rev. Lett.* **78**, 4410 (1997).
21. Note that $I(V)$ cannot be measured over this voltage range without immediately switching the Au adatom.
22. R. Bennewitz *et al*., *Surf. Interface Anal.* **27**, 462 (1999).
23. A. Sanchez *et al*., *J. Phys. Chem. A* **103**, 9573 (1999).
24. W. Hebenstreit *et al*., *Surf. Sci.* **424**, L321 (1999).
25. F. E. Olsson, M. Persson, J. Repp, G. Meyer, http://arxiv.org/abs/cond-mat/0406282.
26. The intrinsic line width of the 6*s*-derived state could not be resolved, because the energy-level spacing is too large in the finite slab calculation.

27. We thank R. Allenspach for valuable comments and K.-H. Rieder for support. We acknowledge partial funding by the European Union projects "AMMIST" and "CHIC," the Swedish Research Council (VR), and the Swedish Strategic Foundation (SSF) through the materials consortium ATOMICS. Allocation of computer resources through the Swedish National Allocation Committee (SNAC) is also gratefully acknowledged.

23 April 2004; accepted 24 June 2004

Total Synthesis of Norzoanthamine

Masaaki Miyashita,* Minoru Sasaki, Izumi Hattori, Mio Sakai, Keiji Tanino

Norzoanthamine, an alkaloid isolated from *Zoanthus* sp., can suppress the loss of bone weight and strength in ovariectomized mice. Norzoanthamine derivatives can also strongly inhibit the growth of P-388 murine leukemia cell lines and human platelet aggregation. However, norzoanthamine's densely functionalized complex stereostructure and scarce availability from natural sources have proved a synthetic challenge. We report the stereoselective total synthesis of norzoanthamine in 41 steps, with an overall yield of 3.5% (an average of 92% yield each step).

The zoanthamine alkaloids, a type of heptacyclic marine alkaloid isolated from colonial zoanthids of the genus *Zoanthus* sp. (*1*–*11*), have attracted much attention from a wide area of science, including medicinal chemistry, pharmacology, natural product chemistry, and synthetic organic chemistry, because of their distinctive biological and pharmacological properties as well as their chemical structures with stereochemical complexity. For example, norzoanthamine (**1**), isolated by Uemura *et al*. in 1995 (*1*–*3*), can suppress the loss of bone weight and strength in ovariectomized mice and has been considered a promising candidate for an antiosteoporotic drug (*3*, *12*), whereas zoanthamine (**2**), isolated by Faulkner *et al*. (*4*, *5*), has exhibited potent inhibitory activity toward phorbol myristate–induced inflammation in addition to powerful analgesic effects (*5*, *6*). Very recently, norzoanthamine derivatives were demonstrated to inhibit strongly the growth of P-388 murine leukemia cell lines, in addition to their potent antiplatelet activities on human platelet aggregation (*13*). Thus, norzoanthamine (**1**) has been studied with keen interest, particularly in relation to the development of a new type of antiosteoporotic drug for use in those advanced in age (*3*, *12*). These distinctive biological properties, combined with novel chemical structures, make this family of alkaloids extremely attractive targets for chemical synthesis (Fig. 1).

However, the chemical synthesis of the zoanthamine alkaloids has remained as an unexplored summit, despite great synthetic efforts (*14*–*27*), owing to their densely functionalized complex stereostructures.

Synthetic challenges posed by norzoanthamine (**1**) and zoanthamine (**2**) include construction of the stereochemically dense C ring that has three adjacent quaternary asymmetric carbon atoms at the C-9, C-12, and C-22 positions; stereoselective synthesis of the ABC carbon framework consisting of the *trans-anti-trans*-fused perhydrophenanthren skeleton; and stereoselective construction of two novel aminoacetal structures, including a bridged δ-lactone.

Division of Chemistry, Graduate School of Science, Hokkaido University, Sapporo 060-0810, Japan.

*To whom correspondence should be addressed. E-mail: miyasita@sci.hokudai.ac.jp